

## Radiative transport at the 184.9-nm Hg resonance line. I. Experiment and theory

H. A. Post\*

*Philips Research Laboratories, P.O. Box 80.000, 5600 JA Eindhoven, The Netherlands*

(Received 22 August 1985)

Measurements are reported of the radiative decay rate of the Hg  $6^1P_1$  population under conditions of strong radiation trapping at the 184.9-nm resonance line. The experiments were made in the afterglow of a low-pressure Hg discharge with a dye-laser absorption method. The radiative decay rate as a function of the Hg pressure shows a pronounced minimum. The value at minimum is lower than the limiting value at higher Hg densities by a factor of 2. Furthermore, the experimental rates are up to a factor of 8 lower than those calculated from theory with the usual assumption of complete redistribution. Indeed, complete redistribution is not expected in the present case, where the optical thickness is large and elastic collision rates are smaller than the single atom spontaneous emission rate. We derived an analytical expression for the fundamental-mode radiative decay rate in a homogeneous medium from a theory based on partial redistribution in frequency. A condition for the existence of a fundamental mode is discussed and is shown to be largely satisfied in our experiments. The expression for the decay rate was obtained for a resonance line with a hyperfine structure, and was elaborated for a cylindrical geometry. The resulting calculated decay rates agree with the experimental ones within 25%.

## I. INTRODUCTION

Imprisonment of resonance radiation<sup>1-7</sup> plays an important role in many systems. Due to this process the escape rate of resonance photons from a gas-filled enclosure can be several orders of magnitude lower than the transition probability for the resonance transition. One of those systems is the low-pressure mercury-noble-gas discharge, which is of practical interest because of its application in fluorescent lamps. In these lamps the Hg resonance radiation at the 253.7- and 184.9-nm uv lines (see Fig. 1) is mainly responsible for the light production.<sup>8</sup> The contribution of the 184.9-nm line to the total uv production can amount to as much as 30%.<sup>8</sup> A calculation of the radiated power at this line requires knowledge of the fundamental mode radiative decay rates caused by the radiation-trapping processes. However, only very limited experimental data are available in literature.<sup>9</sup> Furthermore, no sufficiently accurate theory exists, as is discussed below.

The transport of resonance radiation has been treated by Holstein,<sup>1</sup> Biberman,<sup>2</sup> and others<sup>3,4</sup> on the assumption known as complete redistribution in frequency. This assumption implies that the line profile of the radiation emitted from a given volume element is proportional to the absorption line profile of the medium. The effects of correlations existing between the absorbed and emitted photon frequencies in the individual absorption-reemission events are then supposed to be negligible. This is justified in the limit of many decorrelating collisions (elastic collision rate  $\gamma_c$ ) within a natural lifetime  $\tau_n = 1/\gamma$ , i.e., when  $\gamma_c/\gamma \gg 1$ .<sup>1</sup> It has been shown by Monte Carlo calculations<sup>6</sup> as well as analytically<sup>5,7</sup> that, if, in contrast,  $\gamma_c/\gamma \ll 1$ , the radiative decay after a few natural lifetimes is also predicted well with this assumption in the case that the optical thickness is large and the wings of the Voigt absorption line profile are optically

thin and contribute relatively little to the total emission. This is equivalent to the limiting case of a pure Doppler-broadened absorption line profile. With complete redistribution in frequency the radiative transfer problem depends only upon the optical thickness at the line center and on the absorption line profile. Exact and approximate solutions have been given by many authors.<sup>1-6</sup>

However, sizable deviations from the complete redistribution results occur if the wings of the Voigt absorption line profile are important in the low-collision-rate ( $\gamma_c/\gamma \ll 1$ ), large-optical-thickness regime.<sup>5</sup> An expression for the radiative decay rate in this case also depends explicitly upon the ratio  $\gamma_c/\gamma$ . It has only been given for the rate of the early time escape following pulsed pencil-like excitation along the axis of a cylinder in combination with side-on observation of a slab region around this axis.<sup>5</sup>

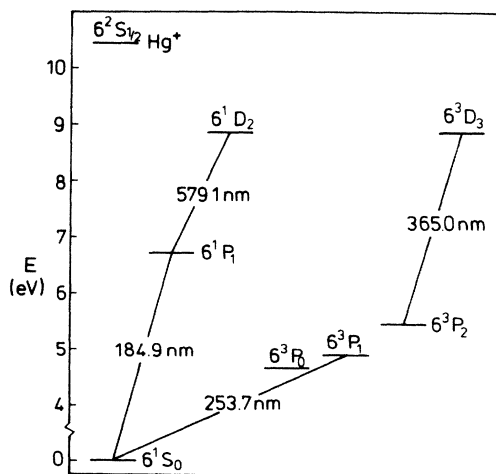


FIG. 1. Simplified energy-level scheme of Hg.

However, in many laboratory experimental situations an expression for the radiative decay rate in the fundamental mode, i.e., at "late times," would be more useful. Such an expression has been lacking up until now.

For the discharge conditions of fluorescent lamp operation, the assumption of complete redistribution in frequency fails for the radiative transport at the 184.9-nm line ( $6^1P_1-6^1S_0$ ). We report measurements of the Hg  $6^1P_1$  population decay in the afterglow of a low-pressure Hg discharge. The decay of this temporary overpopulation in the  $6^1P_1$  level, obtained by the fast switch-off of the discharge (see Sec. III), was measured using a dye-laser absorption method. The experimental setup is described in Sec. II. In Sec. III an analysis is given of the experimental data, and the resulting radiative decay rates are compared with those calculated from theory with the complete redistribution assumption. In Sec. IV a partial redistribution theory is described for the fundamental mode radiative decay rate  $\beta$ , which is an extension of the work of Payne *et al.*<sup>5</sup> The analytical expression for  $\beta$ , obtained for a resonance line with hyperfine structure, is valid for large optical thickness and a vast range of  $\gamma_c/\gamma$  values. A condition for the existence of a fundamental mode is discussed and is shown to be largely satisfied in our experiments. In Sec. V the theory is applied to the case of an infinite cylinder and several results, such as, e.g., the shape of the emission line profile, are considered in more detail. Furthermore, an approximation is discussed which considerably simplifies the calculation of  $\beta$  at the expense of only a small error. In Sec. VI the radiative decay rates calculated using this approximation are compared with those obtained from the experiments. Section VII contains a summary.

## II. EXPERIMENT

The Hg  $6^1P_1$  density in a low-pressure mercury discharge was determined by measuring the absorption at hyperfine components of the 579.1-nm line ( $6^1P_1-6^1D_2$ ); see Fig. 1. From the measured decay of this  $6^1P_1$  density in the afterglow of the discharge, the radiative decay rate of the 184.9-nm resonance line could be derived.

The experimental setup was identical to the one described previously,<sup>9</sup> except for a somewhat different discharge-tube geometry. A summary will be given here. For more details, see Ref. 9. The experiments were made using a U-shaped cylindrical discharge tube, which permitted the measurement of axially averaged  $6^1P_1$  densities. The geometry of the Pyrex tube ensured that the influence of end effects on the axially averaged radiative decay rates were small. The tube had an inner radius  $R$  of 12.5 mm and a middle section of length  $l \approx 0.50$  m. The temperatures of the tube wall,  $T_w$ , and of an appendix,  $T_{Hg}$ , could be controlled independently by water from two thermostats. The appendix served as the coldest spot determining the mercury vapor pressure. Its temperature  $T_{Hg}$  is quoted throughout the paper and was always 1°C lower than  $T_w$ . The mercury consisted of a natural mixture of isotopes. The mercury vapor pressure ranged from 0.17 to 7 Pa and the discharge current  $I$  from 3 to 100 mA. The polarity of the discharge was switched periodically, so that electrophoretic effects<sup>10</sup> had a negligible in-

fluence on the axial number densities. After the initiation of the afterglow, the discharge voltage dropped within 0.2  $\mu$ s to  $\sim 1\%$  of its steady-state value.

The absorption measurements were made using a stabilized single-mode dye laser as a light source. The laser beam traversed the U-shaped discharge tube in the axial direction. The logarithm of the ratio of the transmitted and reference beam intensities was determined by a two-channel boxcar integrator. The  $6^1P_1$  density decay curves recorded in the afterglow of the discharge were stored in a computer data file.

## III. RESULTS AND ANALYSIS

### A. Decay measurements

For the  $6^1P_1$  density decay measurements the laser wavelength was held at the maximum of the absorption coefficient,  $k_m$ , of the even isotope hyperfine component of the 579.1-nm line ( $6^1P_1-6^1D_2$ ).<sup>11</sup> Some examples of the resulting curves of  $k_m(t)l$ , the optical thickness along the discharge axis, are shown in Fig. 2. For  $t \leq 1 \mu$ s the decay curves are affected by the finite boxcar sample time (1  $\mu$ s). We note here that, in the estimates entering the discussions below, we used literature data for the  $6^3P$  densities,<sup>12</sup> the electron density and energy distribution function,<sup>13</sup> and the cross sections for electron impact (de-)excitation at the atomic transitions  $6^1S_0-6^3P_{0,1,2}$  (Ref. 14),  $6^1S_0-6^1P_1$  (Ref. 9), and  $6^3P_{0,1,2}-6^1P_1$  (Ref. 9).

At our low discharge currents the time dependence of the  $6^1P_1$  population in the afterglow is determined by its fundamental mode radiative decay rate  $\beta$  (see Sec. IV), which we want to determine, as well as by the behavior of the  $6^1P_1$  excitation. This excitation will be discussed next. It can be estimated that after the discharge is

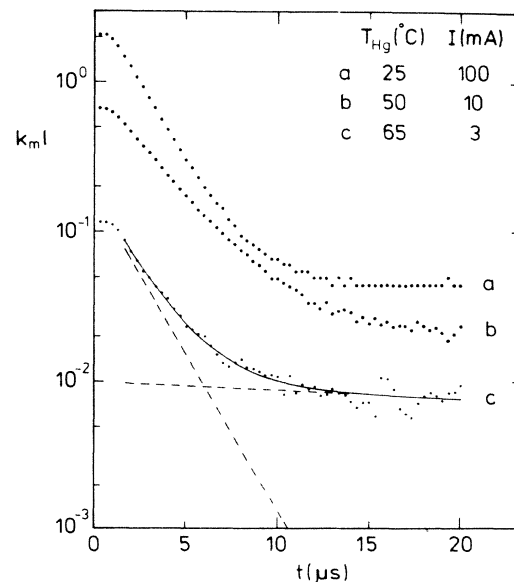


FIG. 2. Time dependence of the optical density measured along the cylinder axis for  $T_{Hg} = 25, 50, \text{ and } 65^\circ\text{C}$ , and  $I \leq I_c$  (see text). The solid line represents the best fit of a sum of two exponentials for  $T_{Hg} = 65^\circ\text{C}$ ,  $I = 3$  mA; the dashed lines denote these two exponentials individually.

switched off the high-energy tail (electron energy  $> 5$  eV) of the electron-energy distribution cools off rapidly with a time constant  $\ll 1 \mu\text{s}$  due to inelastic collisions with ground-state Hg atoms. Therefore, the direct excitation of the excited Hg states decreases very rapidly to a much lower level than in the steady state of the discharge. This can be illustrated by measurements of the 365.0-nm emission from the very-short-lived  $6^3D_3$  level [natural lifetime  $\sim 7.4$  ns (Ref. 15)], which show a fast decay with time constant  $\ll 1 \mu\text{s}$ , followed after  $\sim 2 \mu\text{s}$  by an order of magnitude slower decay. The  $6^1P_1$  level population  $n_{6^1P_1}$ , however, cannot follow the decreasing excitation instantaneously, because its decay time constant  $\beta^{-1}$  is too large [ $> 1 \mu\text{s}$  (Ref. 9)] due to radiation trapping. In this way an overpopulation is created at  $t \approx 2 \mu\text{s}$ .

For the description of  $n_{6^1P_1}(t)$  at sufficiently low discharge currents, the remaining decreasing excitation for  $t \geq 2 \mu\text{s}$  can be approximated well by an exponential function of time with rate  $\beta_1 \ll \beta$ . The radiative deexcitation for  $t \geq 2 \mu\text{s}$  can be described by the fundamental mode radiative decay rate  $\beta$  (see Sec. IV). This is because the radial dependence of the  $6^1P_1$  excitation and therefore of the  $6^1P_1$  density in the steady state of the discharge is already a good approximation to that of the fundamental mode radiative deexcitation rate. This was confirmed by measurements of the radial  $6^1P_1$  density profile; see also Ref. 9 and Sec. IV. Because the same applies in the afterglow, the  $6^1P_1$  density decay curves are given simply as the sum of two exponentials with rate constants  $\beta$  and  $\beta_1$ , respectively.

### B. Radiative decay rate

The values of  $\beta$  and  $\beta_1 \ll \beta$  were obtained from a least-squares fit of a sum of two exponentials to the measured  $n_{6^1P_1}(t)$  curves for  $t \geq 2 \mu\text{s}$  (see Fig. 2), and differed by at least a factor of 10 under all conditions. At a given mercury density  $n_{\text{Hg}}$ ,  $\beta$  was measured as a function of the current  $I$ , and was found to be independent of  $I$  at currents below a certain current  $I_c(n_{\text{Hg}})$ .  $I_c$  decreases with increasing  $n_{\text{Hg}}$  and is larger than 100 mA for  $n_{\text{Hg}} < 3 \times 10^{20} \text{ m}^{-3}$ ; also see Ref. 9. Estimates show that in this current region more than 90% of the  $6^1P_1$  excitation in the steady state of the discharge is due to direct excitation from the  $6^1S_0$  ground state. It follows from the discussion above that this yields a large overpopulation at  $t \approx 2 \mu\text{s}$  (see Fig. 2). Therefore, the approximation of the slow decay of the remaining  $6^1P_1$  excitation by an exponential curve of the same radial dependence as the density in the lowest mode has only a small influence on the accuracy of the fast  $\beta$  values obtained. The values of  $\beta$ , measured at  $I < I_c(n_{\text{Hg}})$ , are shown in Fig. 3 as a function of the mercury density  $n_{\text{Hg}}(T_{\text{Hg}})$ .

The uncertainty of the data is 5%, except at the largest mercury density measured, where it is 20%. At still larger mercury densities the error increased drastically, and no data are presented. This is caused by a decreasing  $I_c$  with increasing  $n_{\text{Hg}}$  and a decreasing  $6^1P_1$  density as a consequence. Moreover, discharge instabilities are present at these low currents (5 mA). Estimates show that

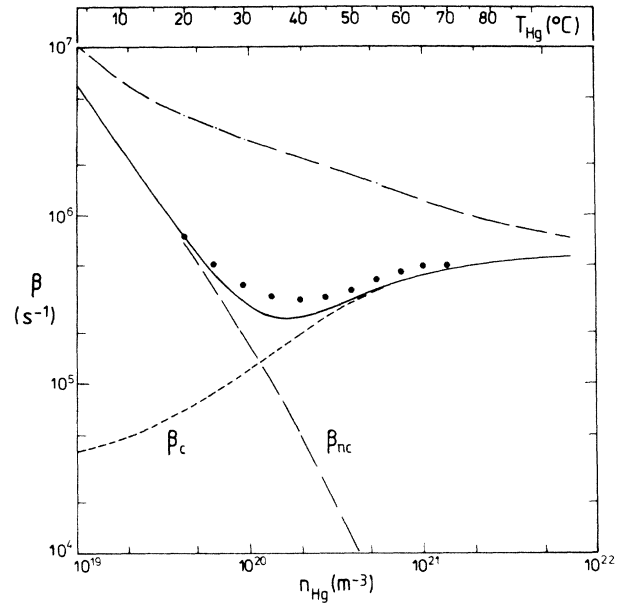


FIG. 3. Fundamental mode radiative decay rate  $\beta$  of the Hg 184.9-nm line as a function of the Hg number density  $n_{\text{Hg}}$  and the coldest spot temperature  $T_{\text{Hg}}$ . The cylinder radius is  $R = 12.5$  mm.  $\bullet$ , experiment; —, present partial frequency redistribution theory, Eq. (20), with radial profile  $f_D(\rho)$ ;  $\beta = \beta_{nc} + \beta_c$ ; see text; theory with assumption of complete frequency redistribution: - - - - -. Both calculations were performed for a natural abundance in the  $6^1P_1$  excited state.

electron-impact depopulation rates are less than 1% of the radiative decay rates  $\beta$ . Atomic collisional depopulation rates contribute less than 1% if cross-section values  $\leq 0.05 \times 10^{-20} \text{ m}^2$  are assumed, which seems reasonable in view of the large energy differences<sup>16</sup> encountered in deexciting the  $6^1P_1$  level (see Fig. 1). Effects of quenching by impurities are negligible since these are removed by the cleaning effect of the discharge.<sup>17</sup> Spectroscopically, no trace of impurities could be detected during the measurements. All  $6^1P_1$  hyperfine levels of the different isotopes<sup>18</sup> have the same decay rate  $\beta$ , and their population is to a good approximation in accordance with the natural abundance.<sup>19</sup> This is due to the strong radiative coupling (see Fig. 4) and was confirmed by absorption measurements at the other hf components of the 579.1-nm line.<sup>11</sup>

The  $\beta$  values for  $0.4 \times 10^{20} \leq n_{\text{Hg}} \leq 2 \times 10^{20} \text{ m}^{-3}$  agree with those of Ref. 9 when allowance is made for a systematic error of  $\sim 10\%$  in the earlier data. This error arose from the tube construction at the ends of the middle section of the tube (“end effects”) and was nearly absent in the present experiment. In this work we have measured  $\beta$  in a much wider range of mercury densities (see Fig. 3).

The radiative decay rate  $\beta$  as a function of the mercury density  $n_{\text{Hg}}$ ,  $\beta(n_{\text{Hg}})$ , shows a pronounced minimum. The minimum value is about 60% of the value at the largest mercury density measured. A minimum in  $\beta(n)$  of the fundamental mode, i.e., at “late times,” has only been observed for the Ne resonance line at 73.6 nm.<sup>20</sup> The early-time escape rate at the 104.8-nm Ar resonance line observed under special experimental conditions also showed a minimum which, however, was less pronounced.<sup>5</sup> We

also calculated  $\beta$  using the complete redistribution theory of Ref. 4 for a Voigt line profile, the hfs of Ref. 18, and a natural abundance in the  $6^1P_1$  excited state. These values, shown also in Fig. 3, are about a factor of 8 larger than our experimental ones and show no minimum as a function of  $n_{\text{Hg}}$ . The occurrence of a minimum in  $\beta(n_{\text{Hg}})$  in a density range where the Voigt absorption line profile varies only slightly clearly shows that  $\beta$  is no function of the optical thickness at line center and of the absorption line shape only. This is in marked contrast with the complete redistribution formulation.

In the next section a theory will be developed which takes into account the important physical processes responsible for the observed behavior of  $\beta(n)$  in the fundamental mode.

#### A. Transport equation

The transport equation for resonance radiation is given by<sup>5</sup>

$$\frac{\partial}{\partial t} N(\rho, x, t) = -\gamma N(\rho, x, t) + S(\rho, x, t) + \gamma k_0 R \pi^{1/2} \int_{-\infty}^{+\infty} dx' \int_V d\rho' N(\rho', x', t) \bar{R}(x', x) \frac{e^{-k(x')R|\rho' - \rho|}}{4\pi|\rho' - \rho|^2}. \quad (1)$$

Here we have neglected the effects of quenching of the excited atoms or absorption by impurity atoms. Furthermore,  $\rho = r/R$  is the reduced spatial position vector, where  $2R$  is the characteristic dimension of the enclosure, i.e., the diameter for a sphere or cylinder and the thickness for a slab. The reduced frequency distance to the line center  $\nu_0$  is given by

$$x = \frac{\nu - \nu_0}{\nu_0} \frac{c}{\bar{v}} \quad \text{where } \bar{v} = (2kT/m)^{1/2},$$

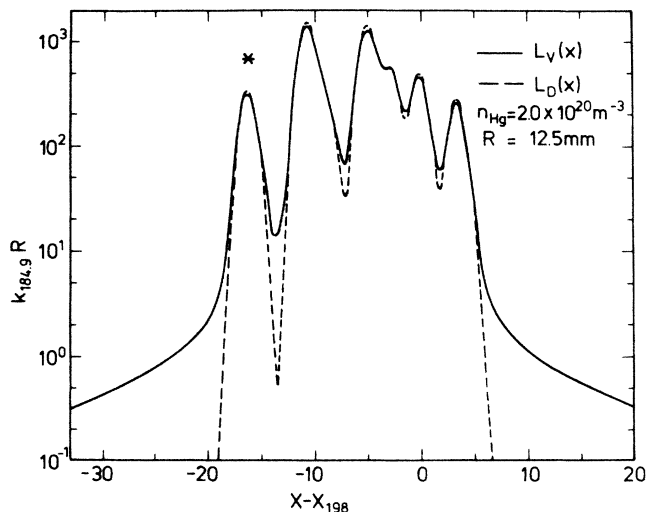


FIG. 4. Absorption coefficient hyperfine structure of the Hg 184.9-nm resonance line for a Voigt and a Doppler line profile of the individual components. The asterisk denotes the  $^{204}\text{Hg}$  line component. The other components represent the isotopes with mass number 202–196.

#### IV. THEORY: GENERAL FORMULATION

In this section we will derive an expression for the radiative decay rate  $\beta$  of a system of excited atoms in its fundamental mode. The expression is obtained for a homogeneous medium and applies for large optical thickness and a vast range of collision rates. A condition is given for the existence of a fundamental mode in this regime. The analytical expression for  $\beta$  is given for a hyperfine structure of the line. The theory starts from the transport equation given by Payne *et al.*<sup>5</sup> and uses an expression for the photon redistribution function<sup>21–26</sup> with an approximation first made by Jefferies and White.<sup>26</sup>

and  $c$ ,  $k$ ,  $T$ , and  $m$  have their usual meanings.

$N(\rho, x, t) dx d\rho$  is the number of excited atoms in  $d\rho$  at  $\rho$  at time  $t$ , which will emit photons into the photon frequency interval  $dx$  at  $x$ , and  $dt \gamma N(\rho, x, t) dx d\rho$  represents the number of photons emitted in  $dt$  from  $d\rho$  into interval  $dx$  at  $x$ . Thus scattering and absorption are taken account of in equal ways;  $\gamma$  is the reciprocal natural lifetime of the excited state.  $S(\rho, x, t) dx d\rho$  is the number of excited atoms in  $d\rho$  at  $\rho$ , which will emit in  $dx$  at  $x$  per unit time, created by processes other than absorption of photons from other parts of the system. The angle-averaged redistribution function  $\bar{R}(x', x)$  is defined such that

$$\bar{R}(x', x) ds k_0 \pi^{1/2} dx$$

represents the probability of a photon of frequency  $x'$  being absorbed (or scattered) while traversing a distance  $ds$  and being reemitted into  $dx$  at  $x$ .  $V$  is the volume containing the excited gas,  $k(x) = k_0 \pi^{1/2} L_V(x)$  is the absorption coefficient, and  $L_V(x)$  is the normalized Voigt absorption line profile given by

$$L_V(x) = \frac{a_v}{\pi^{3/2}} \int_{-\infty}^{+\infty} \frac{e^{-y^2}}{a_v^2 + (x - y)^2} dy, \quad (2a)$$

with

$$a_v = \frac{\lambda_0 \gamma}{4\pi \bar{v}} (1 + \gamma_c / \gamma). \quad (2b)$$

Here,

$$k_0 = \frac{\lambda_0^3 N_0 \gamma}{8\pi^{3/2} \bar{v}} \frac{g_2}{g_1},$$

and for resonance broadening we have, for the elastic collision frequency  $\gamma_c$ ,<sup>27,28</sup>

$$\frac{\gamma_c}{\gamma} = 0.904 \frac{g_2}{g_1} \frac{N_0 \lambda_0^3}{6\pi^2} \zeta, \quad (3)$$

where  $\zeta=1$  for exact resonance and  $\zeta < 1$  for quasiresonance, as occurs in the case of hyperfine structure.<sup>28</sup>  $N_0$  is the number of atoms per unit volume,  $g_2$  and  $g_1$  are the statistical weights of the upper and lower level, respectively, and  $\lambda_0$  is the wavelength at the line center.

Furthermore, we will use the normalized Doppler line profile  $L_D(x)$ ,

$$L_D(x) = \frac{e^{-x^2}}{\sqrt{\pi}}. \quad (4)$$

In the following we will distinguish between the line core ( $|x| \leq x_c$ ) and the line wings ( $|x| \geq x_c$ ). The transition frequency  $x_c > 0$  is defined by the equality of the first two terms in the asymptotic expansion of  $L_V(x)$ , which represent the Doppler and Lorentz contributions to  $L_V(x)$ :  $(1/\sqrt{\pi})e^{-x_c^2} = a_v/\pi x_c^2$ . This yields for  $a_v \ll 1$ , to a good approximation,

$$x_c^2 \simeq \ln \left\{ \frac{\sqrt{\pi}}{a_v} \ln \left[ \frac{\sqrt{\pi}}{a_v} \ln \left[ \frac{\sqrt{\pi}}{a_v} \right] \right] \right\}.$$

### B. Frequency redistribution function

The angle-averaged frequency redistribution function can be written as<sup>21,22,5</sup>

$$\bar{R}(x',x) = (1-P_c)R_{II}(x',x) + P_c R_{III}(x',x), \quad (5a)$$

where

$$P_c = \frac{\gamma_c}{\gamma + \gamma_c} \quad (5b)$$

is the probability that an elastic collision will destroy the correlation between the absorbed and reemitted frequencies in the rest frame of the atoms. The terms with  $P_c$  and  $1-P_c$  give the contribution from the fractions of absorbed photons being reemitted with and without a decorrelating collision before emission. The functions  $R_{II}(x',x)$  and  $R_{III}(x',x)$  obey the sum rule

$$\int_{-\infty}^{+\infty} dx R_{II,III}(x',x) = L_V(x'). \quad (6)$$

For the calculation of radiative decay rates with the use of Eq. (1), the function  $R_{II}(x',x)$  can be approximated by<sup>26,5</sup>

$$R_{II}(x',x) \simeq L_V(x') \{ [1-a(x')]L_D(x) + a(x')\delta(x'-x) \}, \quad (7)$$

with  $a(x) \simeq 0$  for  $|x| \ll x_c$  and  $a(x) \simeq 1$  for  $|x| \gg x_c$ . The first term on the right-hand side of Eq. (7) denotes the full frequency redistribution in the core of the line by the Doppler motion of those atoms which scatter the photon resonantly. The second term expresses the frequency coherence in the wings of the line where the photons are scattered predominantly off resonance by all atoms. The

frequency correlation due to this term causes the coupling of the spatial and frequency dependence in the excited-atom distribution  $N(\rho, x, t)$ . The effect of the  $\delta$ -function approximation upon the calculated values of the decay rate will be discussed later.

The function  $R_{III}(x',x)$ , which corresponds to complete redistribution in the rest frame of the atom, can be approximated by<sup>25,5</sup>

$$R_{III}(x',x) \simeq L_V(x')L_V(x). \quad (8)$$

Using the redistribution function  $\bar{R}(x',x)$  given in Eqs. (5)–(8) in the transport equation (1), the essential redistribution mechanisms for the calculation of the radiative decay rate  $\beta$  are taken into account.

### C. Radiative decay rate

In this subsection we will derive an expression for the radiative decay rate  $\beta$  of a simply connected volume with convex boundary, when the system of excited atoms is in its fundamental mode, i.e., “at late times.” This is quite different from the situation studied by Payne *et al.*,<sup>5</sup> who calculated the early-time escape rate of the resonance radiation in a slab geometry with an excited-atom distribution at  $t=0$  uniform over the midplane  $y=0$  and zero elsewhere. Equations (9)–(14) below are the local versions of the analogous equations given by Payne *et al.*, but with a more general formulation of the geometrical aspects.

The radiative decay rate is the rate at which the energy in the excited-atom density decays by means of radiation transport. We define the local radiative decay rate  $\beta(\rho, t)$  as

$$\beta(\rho, t) \equiv -\frac{1}{N(\rho, t)} \frac{\partial}{\partial t} N(\rho, t), \quad (9)$$

with

$$N(\rho, t) \equiv \int_{-\infty}^{+\infty} dx N(\rho, x, t). \quad (10)$$

Consider the situation where the nonradiative creation term  $S(\rho, x, t) = 0$  for  $t > 0$ . Integration of Eq. (1) over  $x$  yields, with Eq. (9), for  $t > 0$ ,

$$\beta(\rho, t) = \gamma \int_{-\infty}^{+\infty} dx F(\rho, x, t) \eta(\rho, \tau_x, x, t). \quad (11)$$

Equation (11) expresses  $\beta(\rho, t)$  as the integral over all frequencies of the normalized emission line profile,

$$F(\rho, x, t) \equiv \frac{N(\rho, x, t)}{N(\rho, t)}, \quad (12)$$

weighted with the escape function

$$\eta(\rho, \tau_x, x, t) \equiv 1 - \int_V d\rho' \tau_x \frac{e^{-\tau_x |\rho' - \rho|}}{4\pi |\rho' - \rho|^2} \frac{N(\rho', x, t)}{N(\rho, x, t)}. \quad (13)$$

The function  $\eta$  for the net escape of photons with frequency  $x$  from the volume element  $d\rho$  at  $\rho$  depends for given  $\rho, x, t$  on the optical thickness

$$\tau_x \equiv k(x)R,$$

and on the spatial profile at frequency  $x$ ,

$$f(\rho, x, t) \equiv \frac{N(\rho, x, t)}{N(0, x, t)}. \quad (14)$$

For later use, we define

$$g(\rho, \tau_x, x, t) \equiv 1 - \eta(\rho, \tau_x, x, t). \quad (13')$$

From Eqs. (13) it follows that for  $\tau_x \gg 1$  we have  $\eta \ll 1$ , whereas for  $\tau_x \rightarrow 0$  we find  $\eta \rightarrow 1$ . For conditions of strong imprisonment, only a small fraction of the emitted line profile  $F(\rho, x, t)$  is optically thin ( $\tau_x \lesssim 1$ ), so that

$$\frac{\partial}{\partial t} F(\rho, x, t) = -\alpha(\rho, \tau_x, x, t) F(\rho, x, t) + \gamma(1 - P_c) L_D(x) [1 - \beta(\rho, t)/\gamma - \epsilon(\rho, t)] + \gamma P_c L_V(x) [1 - \beta(\rho, t)/\gamma], \quad (15)$$

with

$$\int_{-\infty}^{+\infty} dx F(\rho, x, t) = 1.$$

Here,

$$\epsilon(\rho, t) = \int_{-\infty}^{+\infty} dx a(x) g(\rho, \tau_x, x, t) F(\rho, x, t) \ll 1.$$

Equation (15) is a differential equation for  $F(\rho, x, t)$  in which the second and third terms on the right-hand side act as source terms. These terms depend on time only very weakly through the small corrections  $\beta(\rho, t)/\gamma$  and  $\epsilon(\rho, t)$ , which we shall neglect henceforth [ $\epsilon(\rho, t)$  is of the order  $a_v/\pi x_c$  for  $\tau_x > 1$ ].

The relaxation rate  $\alpha(\rho, \tau_x, x, t)$  of the spectral distribution  $F(\rho, x, t)$  is given by

$$\alpha(\rho, \tau_x, x, t) = \gamma(1 - a(x)(1 - P_c)g(\rho, \tau_x, x, t) - \beta(\rho, t)/\gamma). \quad (16)$$

It is seen from Eq. (16) that in the line core, where  $a(x) \ll 1$ , as well as in the far wing of the line, where  $g \ll 1$ , the spectral relaxation rate attains its maximum value  $\gamma$  to first order in  $\beta/\gamma$  (independent of  $\rho, \tau_x, x, t$ ). This corresponds to complete Doppler redistribution and complete escape, respectively. Furthermore, for  $0 < \eta < 1$ , which one can ascribe to a not too strong variation of  $N(\rho, x, t)$  as a function of  $\rho$ ,  $\alpha$  is always larger than the relaxation rate corresponding to decorrelating collisions,  $\gamma P_c - \beta(\rho, t)$ . This minimum value of  $\alpha$  is attained in the near wing of the line when the optical thickness is so large that the relaxation rate  $\gamma\eta$  due to interaction with other volume elements can be neglected.

For  $P_c = 0$  the different frequency intervals in the line wing act independently, whereas in the line core they are strongly coupled by the Doppler redistribution. In Appendix A 1 it is shown that for  $P_c = 0$  a fundamental mode exists for every wing frequency interval separately,<sup>29</sup> as well as for the line core as a whole, with spatial profiles denoted by  $f^0(\rho, x)$  and  $f_c^0(\rho)$ , respectively. The superscript 0 denotes  $P_c = 0$ ; no superscript will be used for  $P_c > 0$ .

For  $P_c > 0$  all frequency intervals are coupled. After a time sufficiently long for the  $f^0(\rho, x, t)$  and  $f_c^0(\rho, t)$  in the  $P_c = 0$  case to be in their fundamental modes at all  $x$ , the spatial profiles for a nonzero small  $P_c$  value  $f(\rho, x, t)$ , and thus  $\eta$ ,  $g$ , and  $\alpha$ , vary in time only slowly. This slow variation in time is mainly due to a time dependence of the spectral distribution  $F(\rho, x, t)$ , which is caused by the

for not too strong variation of  $N(\rho, x, t)$  with  $\rho$  we find, from Eq. (11),  $\beta(\rho, t) \ll \gamma$ .

In order to attain an expression for  $\beta(\rho, t)$  from Eq. (11), we will concentrate next on obtaining an expression for the emission line profile  $F(\rho, x, t)$ . For this purpose Eq. (1) is transformed into an equation for  $F(\rho, x, t)$ . Using Eqs. (5)–(14) together with Eq. (1), we find, for  $t > 0$ ,

weak coupling of the different spectral regions. However, if the spectral relaxation rate  $\alpha(\rho, \tau_x, x, t)$  is much larger than the decay rate  $\beta(\rho, t)$  for a given  $N(\rho, t)$ , the spectrum  $F(\rho, x, t)$  can adapt itself quasi-instantaneously to the profile  $N(\rho, t)$ . In this case it is reasonable to assume that one fundamental mode exists, in which the spectrum  $F(\rho, x)$ , the spatial profiles  $f(\rho, x)$ , and therefore  $\eta(\rho, \tau_x, x)$ ,  $g(\rho, \tau_x, x)$ , and  $\alpha(\rho, \tau_x, x)$ , are time independent. Obviously,  $\beta$  then does not depend on time and position either, and the decay is exponential with radiative decay rate  $\beta$ . The condition for the existence of a fundamental mode then follows from Eq. (16) if we use the fact that the lower limit of the relaxation rate  $\alpha$  for photons in the wing is found for  $a(x) = 1$  and  $x = x_c$  ( $\tau_{x_c} \equiv \tau_c$ ). The condition becomes

$$P_c + (1 - P_c)\eta(\tau_c) \gg \beta/\gamma. \quad (17)$$

In this inequality we made the approximation

$$\eta(\rho, \tau_c, x_c) \simeq \eta(0, \tau_c, x_c) \equiv \eta(\tau_c).$$

The unknown spatial profile  $f(\rho, x_c)$  at  $x_c$  is called  $f(\rho)$ , so that  $\eta$  at  $\rho = 0$  is only a function of  $\tau_c$ . For the behavior of  $\eta(\tau_c)$  the precise spatial dependence of  $f(\rho, x_c)$  is of minor importance; see Appendix B.

The fundamental mode radiative decay rate  $\beta$  can be found in an iterative way by assuming a function  $f(\rho, x)$ , so that the spectrum  $F(\rho, x)$  is, to first order in  $\beta/\gamma$ , obtained from Eq. (15):

$$F(\rho, x) = \frac{(1 - P_c)L_D(x) + P_c L_V(x)}{1 - (1 - P_c)a(x)g(\rho, \tau_x, x)}, \quad (18)$$

and by varying  $f(\rho, x)$  until the integral

$$\int_{-\infty}^{+\infty} dx F(\rho, x)\eta(\rho, \tau_x, x) = \beta/\gamma \quad (19)$$

is independent of  $\rho$ . In the case of a hyperfine structure with the strengths of the components  $d_i$  given by the natural abundance of the isotopes, an analogous calculation can be made. Taking proper account of the processes for the individual components through Eqs. (12)–(18), we find, for the fundamental mode radiative decay rate of a hyperfine structure (hfs) with a natural abundance in the excited state,

$$\beta_{\text{hfs}} = \gamma \int_{-\infty}^{+\infty} dx \frac{\sum_i (1-P_{c_i}) d_i L_{D_i}(x) + \sum_i P_{c_i} d_i L_{V_i}(x)}{1 - \sum_i a_i(x) (\tau_{x_i}/\tau_x) (1-P_{c_i}) g(\tau_x, x)} \times \eta(\tau_x, x). \quad (20)$$

Here we used detailed-balance relations for the hyperfine structure-mixing collisions due to own gas and foreign gas atoms. The effect of multiplet-mixing collisions due to foreign gas atoms upon the strength of the fluorescence radiation has been treated in Ref. 23. The symbols  $P_{c_i}$ ,  $d_i$ ,  $L_{D_i}(x)$ ,  $L_{V_i}(x)$ ,  $\tau_{x_i}$ , and  $a_i(x)$  denote the same quantities as before, but for the hfs component  $i$ ;  $\tau_x = \sum_i \tau_{x_i}$ . The calculation of  $\eta(\rho, \tau_x, x)$  and therefore of  $\beta$  is done at  $\rho=0$  for convenience. We have defined  $\eta(\tau_x, x) \equiv \eta(0, \tau_x, x)$ .

It is instructive to write expression (20) as

$$\beta_{\text{hfs}} = \beta_{nc} + \beta_c, \quad (21)$$

where the two terms  $\beta_{nc}$  and  $\beta_c$  denote the contributions to  $\beta_{\text{hfs}}$  arising from the source terms without and with a decorrelating collision before emission, respectively.

With increasing density the first term,  $\beta_{nc}$ , decreases, because the optical thickness increases. At low collision rates ( $\gamma_c/\gamma \ll 1 \rightarrow P_c \ll 1$ ) the second term,  $\beta_c$ , increases with increasing density, because the collision rate, and therefore  $P_c$ , also increases. Whereas at very low collision rates the decay rate is mainly determined by the Doppler redistribution— $\beta_{nc}$ —in a large density range, above a certain density the collisional redistribution term  $\beta_c$  dominates. Therefore if this occurs when  $P_c$  is still small,  $P_c \ll 1$ , a minimum is present in the decay rate  $\beta$  as a function of density. Moreover, it follows that in this parameter range the assumption of complete redistribution— $P_c = 1$  in Eqs. (18) and (20)—introduces a large overestimation of  $\beta$  (see Fig. 3).

## V. THEORY: APPLICATION TO AN INFINITE CYLINDER

In this section various aspects of the radiative transport theory given in Sec. IV are considered in more detail. Furthermore, the use of an approximate form of the radial profile  $f(\rho, x)$  is discussed, which considerably simplifies the calculation of  $\beta$ , at the expense of only a small error.

Whereas expressions (1)–(20) are equally valid in plane, cylindrical, and spherical geometry—the difference showing only in  $\eta(\rho, \tau_x, x)$ —we henceforth confine our attention to the case of an infinitely long cylinder. Some quantities to be discussed are calculated at the cylinder axis  $\rho=0$  for convenience, where  $\rho$  is the reduced radial coordinate.

### A. Spectral line shape

We first consider the spectrum  $F(0, x)$ . For simplicity, this is done for a one-component line. The spectrum  $F(0, x)$  is shown in Fig. 5 for the parameter set  $k_0 R = 10^3$  and  $10^4$ ,  $a_v = 0.1$ , and  $P_c = 10^{-3}$ ,  $10^{-2}$ ,  $10^{-1}$ , and 1. The

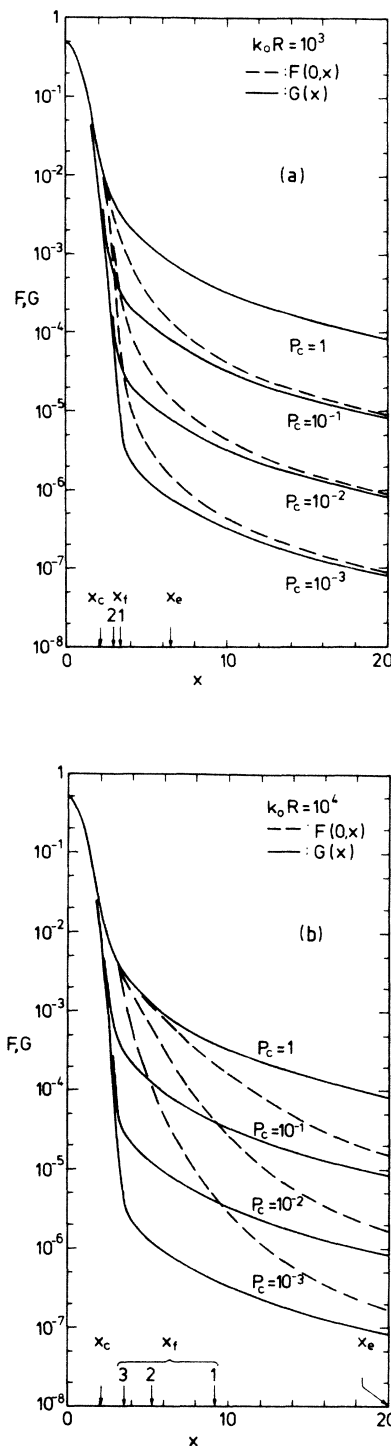


FIG. 5. Line shape functions  $F(0, x)$  and  $G(x)$  for a one-component line with  $a_v = 0.1$ , and  $P_c = 10^{-3}$ ,  $10^{-2}$ ,  $10^{-1}$ , and 1, and the radial profile  $f_D(\rho)$  (see text). For  $P_c = 1$  we have  $F(0, x) = G(x) = L_V(x)$ , the full Voigt line profile; the frequencies  $x_c$ ,  $x_f$ , and  $x_e$  are also shown. The values of  $x_f$  for  $P_c = 10^{-1}$ ,  $10^{-2}$ , and  $10^{-3}$  are denoted by the numbers 1, 2, and 3, respectively. For  $k_0 R = 10^3$  the  $x_f$  values for  $P_c = 10^{-2}$  and  $10^{-3}$  nearly coincide. (a)  $k_0 R = 10^3$ ; (b)  $k_0 R = 10^4$ .

radial profile  $f(\rho, x)$  has been approximated by the frequency-independent profile  $f_D(\rho)$ , which is the radial profile for complete redistribution and a Doppler line shape in the limit of large optical thickness (see Appendix A). The calculation of the escape function  $\eta(\tau_x)$  in this case is described in Appendix B. For  $a(x)$  in the approximation (7) of the redistribution function  $R_{II}(x', x)$  we used the function<sup>5</sup>

$$a(x) = 1 - L_D(x)/L_V(x). \quad (22)$$

Also plotted is the function

$$G(x) \equiv (1 - P_c)L_D(x) + P_c L_V(x),$$

which is the source function in Eq. (15) to first order in  $\beta/\gamma$  and  $\epsilon$ . For  $P_c = 1$  we have  $F(0, x) = G(x) = L_V(x)$ , the full Voigt profile.

It is interesting to compare the spectrum  $F(0, x)$  with the Voigt line profile  $L_V(x)$ , which is the line shape in thermodynamic equilibrium. With Eq. (22), it is found from Eq. (18) that in the line core  $F(0, x)$  is equal to  $L_V(x)$  to a good approximation for  $x \leq x_c$  if  $\eta \ll 1$ . This is analogous to the results of previous calculations.<sup>1,7</sup> In the line wing,  $x > x_c$ , where the relaxation rate terms  $\gamma\eta$  and  $\gamma P_c$  compete, the spectrum  $F(0, x)$  approaches  $L_V(x)$  for those frequencies where the spectral relaxation is dominated by incoherent scattering, i.e.,  $\eta \ll P_c$ . The relative deviation of  $F(0, x)$  from  $L_V(x)$  in this case is  $(1 - P_c)\eta(\tau_x)/P_c$ . These results apply for all  $\rho$  and can be interpreted as follows. At each scattering in the core of the line a spectral redistribution takes place, for a fraction  $1 - P_c$  according to a Doppler profile and for a fraction  $P_c$  according to a Voigt profile. The latter fraction is the main source of supply of photons in the wing,  $x > x_c$ . For  $\eta \ll P_c$  the photons will be trapped in the volume at fixed frequency until they eventually undergo an incoherent scattering. Consequently, a buildup of photon density in the near wing occurs to the full Voigt value, since, on the average,  $1/P_c$  coherent scatterings will take place before an incoherent one. In the far wing, where the medium becomes optically thin ( $\eta \approx 1$ ), no buildup exists and the spectrum approaches the source spectrum  $G(x)$ .

### B. Effective escape function

An interpretation closely related to that in Sec. V A can be given by writing the integrand of Eq. (20) for the one-component line as

$$F(0, x)\eta(\tau_x, x) = G(x)\eta_{\text{eff}}(\tau_x, x), \quad (23)$$

with the effective escape function

$$\eta_{\text{eff}}(\tau_x, x) = \frac{\eta(\tau_x, x)}{1 - (1 - P_c)a(x)g(\tau_x, x)}. \quad (24)$$

Whereas  $\eta(\tau_x, x)$  can be looked upon as the probability for a photon to escape without undergoing any scattering at all,  $\eta_{\text{eff}}$  can be regarded as the probability that a photon escapes before undergoing a frequency-changing scattering. In the line core  $\eta_{\text{eff}}(\tau_x, x) \approx \eta(\tau_x, x)$ , but in the near wing the effective escape function  $\eta_{\text{eff}}(\tau_x, x)$  can be much larger than  $\eta(\tau_x, x)$ . This is due to the frequency correlation in the scattering process by which a wing photon at

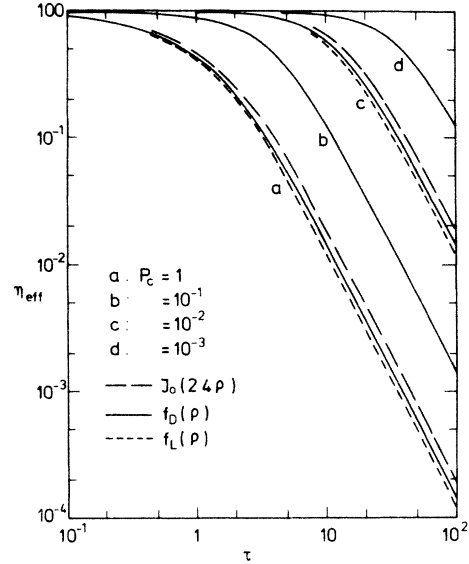


FIG. 6. Effective escape function  $\eta_{\text{eff}}(\tau)$  for  $P_c = 10^{-3}$ ,  $10^{-2}$ ,  $10^{-1}$ , and 1,  $a(x) = 1$ , and the radial profile  $f_D(\rho)$ . For  $P_c = 10^{-2}$  and 1 the curves calculated with the radial profiles  $f_L(\rho)$  and  $J_0(2.4\rho)$  are also shown. For the sake of clarity,  $\eta(\tau)$  from Eq. (29) is not shown here (see text).

frequency  $x$  remains at  $x$  for many coherent scatterings before it is removed from its wing frequency in an incoherent scattering. In Fig. 6,  $\eta_{\text{eff}}(\tau_x, x)$  is plotted for  $a(x) = 1$ , several values of  $P_c$ , and three choices of a frequency-independent radial profile  $f(\rho) = f(\rho, x)$ , so that  $\eta_{\text{eff}}(\tau_x, x)$  is only a function of the optical thickness  $\tau$  at  $x$ :  $\eta_{\text{eff}}(\tau)$ . Note that for  $P_c = 1$  we have  $\eta_{\text{eff}} = \eta$ .

For use in the next section we define  $x_e$  as the frequency at which  $\eta$  reaches the value 0.5 and  $x_f$  as the frequency at which  $\eta_{\text{eff}}$  reaches that value. Simple relations can be derived for some quantities at the frequencies  $x_e$  and  $x_f$ . We find, for the spectral density at  $x_e$ ,

$$F(0, x_e) \approx \begin{cases} L_V(x_e), & 0 < x_e < x_c \\ \frac{2}{1 + P_c} P_c L_V(x_e), & x_c < x_e \end{cases} \quad (25a)$$

$$F(0, x_e) \approx \begin{cases} L_V(x_e), & 0 < x_e < x_c \\ \frac{2}{1 + P_c} P_c L_V(x_e), & x_c < x_e \end{cases} \quad (25b)$$

For the escape function at  $x_f$  we find

$$\eta_{x_f} \equiv \eta(\tau_{x_f}, x_f) \approx \begin{cases} \eta(\tau_{x_e}, x_e) = 0.5, & 0 < x_f \approx x_e < x_c \\ \frac{P_c}{1 + P_c}, & x_c < x_f \leq x_e \end{cases} \quad (26a)$$

$$\eta_{x_f} \equiv \eta(\tau_{x_f}, x_f) \approx \begin{cases} \eta(\tau_{x_e}, x_e) = 0.5, & 0 < x_f \approx x_e < x_c \\ \frac{P_c}{1 + P_c}, & x_c < x_f \leq x_e \end{cases} \quad (26b)$$

Using the relations (26) together with Eq. (18), we find, for the spectral density at  $x_f$ ,

$$F(0, x_f) = \frac{G(x_f)}{2\eta_{x_f}} \approx \begin{cases} L_V(x_f), & 0 < x_f \approx x_e < x_c \\ \frac{1 + P_c}{2} L_V(x_f), & x_c < x_f \leq x_e \end{cases} \quad (27a)$$

$$F(0, x_f) = \frac{G(x_f)}{2\eta_{x_f}} \approx \begin{cases} L_V(x_f), & 0 < x_f \approx x_e < x_c \\ \frac{1 + P_c}{2} L_V(x_f), & x_c < x_f \leq x_e \end{cases} \quad (27b)$$

From Eq. (26b) together with Eq. (B8) we obtain, for  $x_c < x_f \leq x_e$ , the approximate relation between  $\tau_{x_f}$  and  $P_c$ :

$$\tau_{x_f} \simeq 1.2 / (P_c)^{1/2}. \quad (28)$$

### C. Integrand of expression for $\beta$

For the exact calculation of  $\beta$ , the necessary solution for the radial profile  $f(\rho, x)$  can be found by the iteration method discussed in regard to Eqs. (18) and (19). Such a solution will not be attempted here to completion. Instead, we shall go through the first step of this scheme, i.e., we make a reasonable choice of  $f(\rho, x)$  and show the relative insensitivity of  $\beta$  for the specific choice of  $f(\rho, x)$ .

For this purpose, we next discuss the behavior of the integrand (23) of the integral expression (20) for  $\beta$ . This integrand is plotted in Fig. 7 for a one-component line, the same set of  $a_v$ ,  $k_0 R$ , and  $P_c$  as in Fig. 5, and a few choices of a frequency-independent radial profile  $f(\rho)$ , which are discussed in Appendix A 2. The values of  $x_c$ ,  $x_e$ , and  $x_f$  are also shown. It is seen that the integrand attains its maximum near  $x_f$ . This is analogous to the case of complete redistribution, which is attained in our formalism as the special case of  $P_c = 1$ , giving  $\eta_{\text{eff}} = \eta$  and  $x_f = x_e$ . Furthermore, it is seen from Fig. 7 that, for the calculation of  $\beta$ , knowledge of the precise form of the radial profile  $f(\rho, x)$  is mainly important for  $x$  near  $x_f$ .

To obtain an estimate of  $f(\rho, x)$  near  $x_f$ , which can be used in a first approximation at all  $x$  in the calculation of the integrand, we will next discuss the radial profile  $f(\rho, x)$ .

### D. Radial profile $f(\rho, x)$

Using expressions (12), (14), (16), and (18) we find, for the radial profile  $f(\rho, x)$  in the fundamental mode,

$$f(\rho, x) = \frac{\alpha(0, \tau_x, x) N(\rho)}{\alpha(\rho, \tau_x, x) N(0)}.$$

In the most general situation— $x_c < x_f < x_e$ —four spectral regions can be distinguished for  $f(\rho, x)$ :

(a) The core of the line:  $0 < x < x_c$ ,  $a(x) \ll 1$ ,  $g \simeq 1$ ;  $f(\rho, x) \equiv f_c(\rho)$ , independent of  $x$ , corresponding to complete Doppler redistribution.

(b) The near wing of the line:  $x_c < x < x_f$ ,  $a(x) \simeq 1$ ,  $g \simeq 1$ ;  $f(\rho, x) \simeq f_c(\rho)$ , independent of  $x$ , due to redistribution through incoherent scattering only.

(c) The middle wing of the line:  $x_f < x < x_e$ ,  $a(x) \simeq 1$ ,  $g \simeq 1$ ;  $f(\rho, x)$  is a function of  $x$  and is determined at each  $x$  by the (source) function  $f_c(\rho)$  as well as by  $P_c$  and  $\tau_x$ .

(d) The far wing of the line:  $x > x_e$ ,  $a(x) \simeq 1$ ,  $g \ll 1$ ;  $f(\rho, x) \simeq f_c(\rho)$ , independent of  $x$ , since for the emitted photons the medium is optically thin.

The radial profile  $f(\rho, x)$  is always broader than the diffusion profile  $J_0(2.405\rho)$ , and we assume  $f(\rho, x_f)$  to be not much broader than  $f_L(\rho)$  (see Appendix A). For the calculation of  $\beta$ , we then approximate  $f(\rho, x)$  at all  $x$  by  $f_D(\rho)$ , which lies in between  $J_0(2.405\rho)$  and  $f_L(\rho)$ , in this way smoothly joining the regime of complete Doppler redistribution. Here,  $f_L(\rho)$  and  $f_D(\rho)$  are the radial profiles for complete redistribution and a Lorentz and

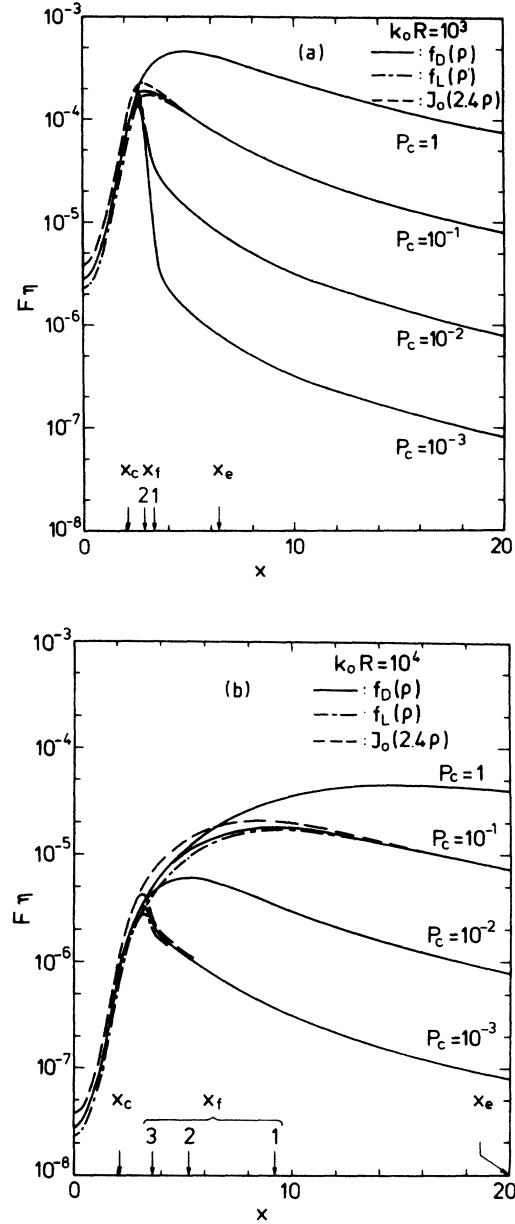


FIG. 7. Integrand of Eq. (20),  $F\eta$ , as a function of  $x$  for a one-component line with  $a_v = 0.1$ ,  $P_c = 10^{-3}$ ,  $10^{-2}$ ,  $10^{-1}$ , and 1, and the radial profile  $f_D(\rho)$ . For  $P_c = 10^{-3}$  and  $10^{-1}$  the curves calculated with the radial profiles  $f_L(\rho)$  and  $J_0(2.4\rho)$  are also shown; the frequencies  $x_c$ ,  $x_f$ , and  $x_e$  are also shown. The values of  $x_f$  for  $P_c = 10^{-1}$ ,  $10^{-2}$ , and  $10^{-3}$  are denoted by the numbers 1, 2, and 3, respectively. For  $k_0 R = 10^3$  the  $x_f$  values for  $P_c = 10^{-2}$  and  $10^{-3}$  nearly coincide. (a)  $k_0 R = 10^3$ ; (b)  $k_0 R = 10^4$ .

Doppler line profile, respectively.

For these frequency-independent radial profiles the escape function at the cylinder axis only depends on the optical thickness  $\tau_x$ :  $\eta(\tau_x, x) = \eta(\tau_x)$ . The calculation of  $\eta(\tau_x)$  for the radial profiles  $f_D(\rho)$ ,  $f_L(\rho)$ , and  $J_0(2.405\rho)$  is described in Appendix B. The resulting curves of  $\eta(\tau_x)$

are shown in Fig. 6. Using the  $\eta(\tau_x)$  functions for  $f_D(\rho)$  and  $f_L(\rho)$  in Eq. (20), we have checked that for the case of complete redistribution ( $P_c = 1$ ) and a one-component line in the limit of large optical thickness, the analytical results of Ref. 4 for  $\beta$  are reproduced within 1% or better for any Voigt profile ( $a_v \geq 0$ ). It has been shown in Ref. 4 that, for a general Voigt line profile  $L_V(x)$  and complete redistribution in frequency [Eq. (20) with  $P_c = 1$ ], values of  $\beta$  with 10% accuracy are obtained with  $\eta(\tau_x)$  given by

$$\eta(\tau_x) = 1 - \frac{\tau_x}{\frac{5}{8}\pi} \arctan \left( \frac{\frac{5}{8}\pi}{\tau_x} \right). \quad (29)$$

The values of  $\eta(\tau_x)$  from (29) are now shown in Fig. 6 for the sake of clarity. For  $\tau_x \lesssim 1.5$  they are larger than  $\eta(\tau_x)$  for the radial profile  $f_D(\rho)$ , with a maximum difference of 5% at  $\tau_x \simeq 0.6$ . For  $\tau_x \gtrsim 1.5$  they are smaller than  $\eta(\tau_x)$  for  $f_D(\rho)$ , with a maximum absolute difference of 10%, independent of  $\tau_x$  for  $\tau_x \gtrsim 3$ .

The radiative decay rate  $\beta$  cannot be calculated from Eq. (20) using the escape function for  $f_D(\rho)$ . The error in  $\beta$  due to this approximation can be estimated from the results obtained with the escape functions for  $J_0(2.405\rho)$  and  $f_L(\rho)$ .

## VI. COMPARISON AND DISCUSSION

The fundamental mode radiative decay rate  $\beta$  for the 184.9-nm Hg line was calculated on the assumption of a natural abundance in the  $6^1P_1$  excited state and is shown in Fig. 3. The condition (17) for the existence of a fundamental mode is largely satisfied:  $P_c + \eta(\tau_c) > 100(\beta/\gamma)$  for all experiments. The contributions  $\beta_{nc}$  and  $\beta_c$ , in Eq. (20), as well as the results for the complete redistribution assumption [ $P_c = 1$  in Eq. (20) and  $\eta(\tau_x)$  from Eq. (29)], are also given. The latter  $\beta$  values can be as much as a factor of 8 larger than our experimental rates. The values obtained with the present theory [Eq. (20) with  $P_c$  given by Eq. (5b)] are in much better agreement, differing by at most 25% from experiment. For  $a(x)$  we used the expression in Eq. (22).

The escape function  $\eta$  was calculated with the frequency-independent radial profile  $f_D(\rho)$  for all mercury densities (see Sec. VD). For  $n_{\text{Hg}} < 2 \times 10^{20} \text{ m}^{-3}$ ,  $f_D(\rho)$  is a good approximation. For  $n_{\text{Hg}} \geq 2 \times 10^{20} \text{ m}^{-3}$  the influence of the uncertainty in  $f(\rho)$  is small:  $f(\rho)$  equal to  $J_0(2.405\rho)$  or  $f_L(\rho)$  leads to 7% higher or 4% lower  $\beta$  values, respectively, whereas the values obtained with  $\eta(\tau_x)$  from the analytical expression (29) are  $< 3\%$  lower.

The atomic data used for the calculations are the natural lifetime  $\tau_n = 1.31 \text{ ns}$  (Ref. 30) and the hyperfine structure of the line.<sup>18,19</sup> The Voigt line profile was calculated using the routine given in Ref. 31. The optical thickness at the axis of the cylinder  $\tau_x = k(x)R$  is shown in Fig. 4 for the complete Voigt line as well as the Doppler line profiles of the hfs, and  $n_{\text{Hg}} = 2 \times 10^{20} \text{ m}^{-3}$ . This figure also gives a good impression of the situation in the whole range of experimental conditions reported, since  $a_v$  changes less than  $\sim 10\%$ .

For the Hg collisional broadening we used the theory of Ref. 27 for resonant collisions. In our case, where the hy-

perfine interaction is not small enough to be neglected during the collision (see Omont and Meunier<sup>27</sup>), this theory applies only for the even Hg isotopes (70% of the total Hg density<sup>19</sup>), which have zero nuclear spin. We assumed that the broadening for the hf levels of the odd Hg isotopes, which have nonzero nuclear spin, is equal to that for the even ones. Using Eq. (3) with  $\zeta = 1$ , we find, for  $P_c$  from Eq. (5b),

$$P_c = \frac{0.029 \times n_{\text{Hg}}}{1 + 0.029 \times n_{\text{Hg}}}, \quad n_{\text{Hg}} \text{ in } 10^{20} \text{ m}^{-3}.$$

The use of the theory of Ref. 28 for quasiresonant collisions, which also applies for the even isotopes only, would yield an averaged 15% lower collision rate for the total hfs [ $\zeta = 0.85$  in Eq. (3)], on the same assumption as used above. This would have resulted in values of the decay rate  $\beta$  which, for mercury densities of  $4 \times 10^{19}$ ,  $2 \times 10^{20}$ , and  $1 \times 10^{21} \text{ m}^{-3}$ , are only 1%, 13%, and 11% lower than those obtained with  $\zeta = 1$ .

Our use in the theory of the angle-averaged redistribution function limits its application to cases of strong imprisonment, where the absorbed emission comes nearly equally from all directions, so that the emission is approximately isotropic. The redistribution function given in Eq. (5) has been calculated quantum mechanically<sup>22</sup> for foreign gas broadening in the rest frame of the atom. The expressions for  $R_{\text{II}}(x',x)$  and  $R_{\text{III}}(x',x)$  in the laboratory frame<sup>24-26</sup> are rather complicated. The more simple expressions (7) and (8) used in our theory in Sec. IV are approximations. It is argued in Ref. 5 that, with  $\gamma_c/\gamma$  given by Eq. (3) and using Eq. (8) for  $R_{\text{III}}(x',x)$ , Eq. (5) should also hold for self-broadening. The approximation of  $R_{\text{III}}(x',x)$  by Eq. (8) is best when used for large values of  $|x'|$  or  $|x|$ ,<sup>5,25</sup> i.e., at large optical thickness where the wings dominate the radiation transport process. For the wings of a hfs of overlapping line components, this approximation is even better justified than for a single line, because on the average the frequency distance to the line center of the hf components is larger.

In the approximation of  $R_{\text{II}}(x',x)$  by Eq. (7), the use of the first term also requires strong imprisonment:  $k_0 R \geq 50$ .<sup>5</sup> The effect of the approximation of the second term by a  $\delta(x'-x)$  function<sup>26</sup> is discussed in more detail in Appendix C. With this Jefferies-White approximation the decay rate  $\beta$  is underestimated if the line wing is optically thick and the collision rate low ( $P_c \ll 1$ ). The introduced error in  $\beta$  is estimated in Appendix C to be largest when  $\beta_{nc}$  and  $\beta_c$  of Eq. (21) are about equal, i.e., near the minimum in  $\beta(n_{\text{Hg}})$ . This is confirmed by our data in Fig. 3. From a rough estimation we find in Appendix C that at  $n_{\text{Hg}} = 1.5 \times 10^{20} \text{ m}^{-3}$  the decay rate  $\beta$  is underestimated by about 30% owing to the use of the JW approximation. We feel that the observed maximum difference of 25% between experiment and theory around the minimum in  $\beta(n_{\text{Hg}})$  is due, at least for a large part, to the JW approximation in  $R_{\text{II}}(x',x)$ , although the good agreement with the estimated error is fortuitous because of the roughness of the estimation. The use of the JW approximation then predicts a somewhat too pronounced minimum in  $\beta$  as a function of density. This has also

been found for the early-time escape rate of Ar resonance radiation.<sup>5</sup>

The range of  $P_c$  values where expression (20) applies is mainly determined by the condition (17) for the existence of a fundamental mode in the JW approximation. It can be shown that for  $k_0 R \geq 50$  and  $a_v \ll 1$  we have  $P_c \gg \beta_c / \gamma$ . We then find that condition (17) is satisfied, for all  $P_c$  if

$$(1 - P_c)\eta(\tau_c) \gg \beta_{nc} / \gamma$$

and for  $P_c \gg \beta_{nc} / \gamma$  if

$$(1 - P_c)\eta(\tau_c) \gg \beta_{nc} / \gamma.$$

For a single-line component,  $\eta(\tau_c)$  can be easily estimated, using  $\tau_c \simeq 0.1 k_0 R a_v$ .

## VII. SUMMARY AND CONCLUSIONS

Measurements are reported of the effective radiative decay rate of the Hg  $6^1P_1$  overpopulation under conditions of strong radiation trapping at the 184.9-nm line. The measurements were made in the afterglow of a low-pressure Hg discharge using a dye-laser absorption method to detect the Hg  $6^1P_1$  density decay. The decay rate as a function of Hg density shows a pronounced minimum. The experimental rates are up to a factor of 8 lower than those calculated from theory with the assumption of complete redistribution in frequency. From a theory based on partial redistribution in frequency, we derived an expression for the radiative decay rate in the fundamental mode for spherical, cylindrical, and slab geometry. The analytical expression obtained for a homogeneous medium is valid at large optical thickness in a wide range of  $\gamma_c / \gamma$  values and also applies for a hyperfine structure of the resonance line. A condition is given for the existence of a fundamental mode and is shown to be largely satisfied in our experiments. The rates calculated with this expression agree within 25% with our experimental data obtained for the Hg  $6^1P_1$  population decay rate.

In paper II (Ref. 32) (following paper) an extensive series of experiments will be reported, which allows a comparison between theory and experiment for a much wider range of experimental conditions.

## ACKNOWLEDGMENTS

The author is indebted to Dr. Q. H. F. Vreken for a thorough reading of the manuscript, many suggestions for its improvement, and discussions. Thanks are also due to Dr. C. van Trigt for discussions.

## APPENDIX A: SPATIAL PROFILE $f(\rho, x)$

In this appendix the spatial profile  $f(\rho, x)$  in the fundamental mode is discussed in more detail for the case of an infinitely long cylinder. For a plane or spherical geometry analogous expressions can be obtained.

### 1. $P_c = 0$

Consider in the redistribution function approximation of Eqs. (5), and (7) and (8), the case where  $P_c = 0$ , and assume that a spatial distribution of excited atoms exists, created at  $t = 0$  in such a way that the spectral distribution is nonzero in the optically thick wings ( $\tau_{x_c} \gg 1$ ). For  $x > x_c$  this situation is completely analogous to the "one-speed" (or "constant-cross-section") approximation in the neutron transport theory.<sup>29</sup> The results of this theory show that the radial profile  $f^0(\rho, x)$  for  $0 < \rho < 1 - 1/\tau_x$  is given to a good approximation by the solution of a diffusion equation with the boundary condition  $f^0(1 + 0.71/\tau_x, x) = 0$ . The superscript 0 denotes the very special situation of  $P_c = 0$ ; no superscript is used for  $P_c > 0$ , as occurs in real physical situations.

Therefore, a fundamental mode exists for each  $x > x_c$  independently, with the radial profile

$$f^0(\rho, x) \simeq J_0 \left[ \frac{2.405}{1 + 0.71/\tau_x} \rho \right],$$

$$x > x_c, \quad 0 < \rho < 1 - 1/\tau_x. \quad (\text{A1a})$$

It follows that  $f^0(\rho, x)$  is always broader than  $J_0(2.405\rho)$ , the fundamental mode diffusion profile with its first zero at the wall. For  $\tau_x \gg 1$  the differences, however, are very small. For the line core an analogous situation would exist, were it not for the Doppler redistribution exerting a strong coupling for all  $x$  with  $0 < x < x_c$ . We therefore expect the line core to act as a whole in a fundamental mode behavior with the radial profile  $f_c^0(\rho)$  independent of  $x$  and given by

$$J_0(2.405\rho) \leq f_c^0(\rho) \leq J_0 \left[ \frac{2.405}{1 + 0.71/\tau_{x_c}} \rho \right],$$

$$x \leq x_c, \quad 0 < \rho < 1 - 1/\tau_{x_c}. \quad (\text{A1b})$$

### 2. $P_c > 0$

Now let  $P_c$  become nonzero,  $P_c > 0$ : Then there exists a certain coupling between the different frequency intervals which will yield spatial distributions different from Eq. (A1). Because the  $f^0(\rho, x)$  are for all  $x$  broader than  $J_0(2.405\rho)$ , this will remain valid for  $f(\rho, x)$ . In the line core,  $f_c(\rho)$  will become broader due to the coupling to frequency regions with broader  $f^0(\rho, x)$ . Because  $f^0(\rho, x)$  is broader for larger  $x$ , it can be expected that the strongest influence on the broadening of  $f_c(\rho)$  comes from  $x \simeq x_f$ , where  $\eta_{\text{eff}} \simeq 0.5$ . This comes about since for  $x > x_f$  the photons mostly escape before a frequency-changing scattering occurs:  $\eta_{\text{eff}}(\tau_x, x) > \eta_{\text{eff}}(\tau_{x_f}, x_f) = 0.5$ ; moreover, their generation rate decreases:  $G(x) < G(x_f)$ . For  $x_c < x < x_f$  the opposite is true. We then find

$$J_0(2.405\rho) \leq f(\rho, x) \leq J_0 \left[ \frac{2.405}{1 + 0.71/\tau_x} \rho \right],$$

$$0 < x < x_f, \quad 0 < \rho < 1 - 1/\tau_x. \quad (\text{A2})$$

Therefore, if  $P_c \ll 1$ , then  $\tau_{x_f} \gg 1$ , and  $f(\rho, x_f)$  and  $f_c(\rho)$

are given to a good approximation by the narrowest possible profile:  $f(\rho, x_f) \simeq f_c(\rho) \simeq J_0(2.405\rho)$ . If  $P_c$  increases,  $\tau_{x_f}$  decreases, and  $f_c(\rho)$  and  $f(\rho, x_f)$  become broader.

To what extent  $f_c(\rho)$  is broadened can be seen best from the situation of complete redistribution ( $P_c = 1$ ), where  $\tau_{x_f}$  is smallest  $\tau_{x_f} = \tau_{x_e} \simeq 1$ , and  $f(\rho, x_f) = f_c(\rho) = f(\rho)$ . In this case<sup>4</sup> the spatial profiles  $f_D(\rho)$  and  $f_L(\rho)$  for a Doppler and Lorentz line shape, respectively, are both broader than  $J_0(2.405\rho)$ . For a Voigt line shape the spatial profile  $f_V(\rho)$  will be in between  $f_D(\rho)$  and  $f_L(\rho)$ , depending on the values of  $a_V$  and  $k_0R$ . Although the fraction of emitted photons per unit optical thickness with  $\tau_x \simeq 1$  is much larger for a Lorentz than for a Doppler line shape,  $f_L(\rho)$  is still only 10% larger than  $f_D(\rho)$ , except very close to the wall. It follows that the influence of the photon fraction with  $\tau_x \simeq \tau_{x_f}$  upon the broadening of  $f_c(\rho)$  is not very large.

Thus we have found the following for the radial profile at  $x_f$ ,  $f(\rho, x_f)$ .

(i) If  $x_f > x_c$ ,  $f(\rho, x_f) \simeq f_c(\rho)$  in the limits of both  $P_c \ll 1$  and  $P_c \simeq 1$ . We assume that it will not be much broader than  $f_c(\rho)$  for all  $P_c$  values. In fact, we will assume that  $f(\rho, x_f)$  is not much broader than  $f_L(\rho)$ .

(ii) If  $x_f \simeq x_c < x_e$ ,

$$f(\rho, x_f) = f_c(\rho) \simeq J_0 \left[ \frac{2.405}{1 + 0.71/\tau_c} \rho \right] < f_D(\rho),$$

since the broadening influence of line-wing photons decreases.

(iii) If  $x_f = x_e < x_c$ ,  $f(\rho, x_f) = f_c(\rho) \simeq f_D(\rho)$ , since the line wings are optically thin.

In all cases,  $f(\rho, x_f)$  is broader than  $J_0(2.405\rho)$ .

## APPENDIX B: CALCULATION OF ESCAPE FUNCTION $\eta(\tau)$

In this appendix we will calculate the escape function  $\eta(\tau)$  at the axis of an infinitely long cylinder for a given spatial profile  $f(\rho)$ ,

$$\eta(\tau) = 1 - \int_V d\rho' \tau \frac{e^{-\tau|\rho'|}}{4\pi|\rho'|^2} f(\rho'). \quad (\text{B1})$$

In a coordinate system with the spherical coordinates  $\rho'$ ,  $\theta$ , and  $\varphi$  ( $\theta$  is the angle between  $\rho'$  and the cylinder axis, and  $\varphi$  is the angle in the  $\theta = \pi/2$  plane) and the origin at the cylinder axis,  $\eta(\tau)$  can be written as

$$\eta(\tau) = 1 - \int_0^{\pi/2} d\theta \sin\theta \int_0^{1/\sin\theta} d\rho' \tau e^{-\tau\rho'} f(\rho' \sin\theta). \quad (\text{B2})$$

Here we have used the cylindrical symmetry of the problem, which implies that  $f(\rho')$  is an even function of  $\rho \equiv \rho' \sin\theta$ . The integral in (B2) can be simplified by an approximation of  $f(\rho)$  by a power series of a large but finite number of terms. With the boundary conditions  $f(0) = 1$  and  $f(1) = 0$ , we find

$$f(\rho) = \sum_{n=1}^{n_{\max}} a_{2n} (1 - \rho^{2n}), \quad (\text{B3a})$$

$$\sum_{n=1}^{n_{\max}} a_{2n} = 1. \quad (\text{B3b})$$

This gives

$$\eta(\tau) = \sum_{n=1}^{n_{\max}} a_{2n} \eta_{2n}(\tau), \quad (\text{B4})$$

with

$$\begin{aligned} \eta_{2n}(\tau) &= 1 - \int_0^{\pi/2} d\theta \sin\theta \int_0^1 d\rho \frac{\tau}{\sin\theta} e^{-\rho\tau/\sin\theta} (1 - \rho^{2n}) \\ &= \int_0^{\pi/2} d\theta \sin\theta I_{2n}(\tau/\sin\theta), \end{aligned} \quad (\text{B5a})$$

$$I_{2n}(\sigma) = \frac{(2n)!}{\sigma^{2n}} - \sum_{k=1}^{2n} \frac{(2n)!}{(2n-k)!} \frac{e^{-\sigma}}{\sigma^k}. \quad (\text{B5b})$$

Equation (B5b) was obtained from Ref. 33. In this way  $\eta_{2n}(\tau)$  and therefore  $\eta(\tau)$  can be obtained from Eqs. (B5) by numerical quadrature. However, for small  $\tau$ , i.e., small  $\sigma$ , and large  $n$ , loss of significant figures occurs due to cancellation of terms. By expansion of  $e^{-\sigma}$  in its power series, it can be shown that all terms with  $1/\sigma^k$ ,  $k > 0$ , in  $I_{2n}(\tau)$  cancel, leaving

$$I_{2n}(\sigma) = \sum_{j=0}^{\infty} c_{2n,j} (-\sigma)^j, \quad (\text{B6})$$

$$c_{2n,j} = \sum_{l=0}^{2n-1} \frac{(-1)^l (2n)!}{(2n-1-l)!(j+1+l)!}.$$

In the calculation of  $\eta_{2n}(\tau)$ , Eq. (B5b) was used for  $\sigma \geq 1$  and Eq. (B6) for  $\sigma < 1$ . In the limit of large  $\tau$  we find, from Eqs. (B4) and (B5),

$$\eta(\tau) \simeq a_2 \eta_2(\tau) = \frac{4}{3} \frac{a_2}{\tau^2}. \quad (\text{B7})$$

We are left with the determination of the power series which describe the radial profiles  $f_D(\rho)$ ,  $f_L(\rho)$ , and  $J_0(2.405\rho)$  sufficiently well. It turns out that these profiles can be approximated within less than 1% by the expression

$$f(\rho) = \sum_{n=1}^3 a_{2n} (1 - \rho^{2n}) + \left[ 1 - \sum_{n=1}^3 a_{2n} \right] (1 - \rho^8),$$

with the coefficients  $a_{2n}$  given in Table I. The coefficients  $a_2$ , which determine the behavior of  $\eta(\tau)$  for large  $\tau$ , can be determined with good accuracy from Ref. 4 ( $f_D$ ,  $f_L$ ) and Ref. 34 ( $J_0$ ), respectively. The coefficients  $a_4$  and  $a_6$  were obtained by a least-squares fit ( $a_8 = 1 - a_2 - a_4 - a_6$ ).

For use in Sec. VB, we note that the curves of  $\eta(\tau)$  shown in Fig. 6 are described within 30% for all  $\tau$  by the function

$$\eta(\tau) = \frac{1}{0.7\tau^2 + 1}. \quad (\text{B8})$$

TABLE I. Coefficients of the power series expansion  $\sum_{n=1}^4 a_{2n}(1-\rho^{2n})$  for the radial profiles  $f_L(\rho)$ ,  $f_D(\rho)$ , and  $J_0(2.405\rho)$ .

	$a_2$	$a_4$	$a_6$	$a_8$
$f_L(\rho)$	0.8983	0.3028	-1.6008	1.3997
$f_D(\rho)$	1.0712	-0.0109	-0.7878	0.7275
$J_0(2.405\rho)$	1.4450	-0.5212	0.0799	-0.0037

It is illustrative to see that the decay rate at large optical thickness  $\tau$  for the  $J_0(2.405\rho)$  radial profile obtained from Eq. (B7) and  $a_2$  from Table I is exactly equal to the rate  $\nu_d$  obtained from the diffusion equation with boundary conditions

$$\frac{d^2f}{d\rho^2} + \frac{1}{\rho} \frac{df}{d\rho} + \frac{\nu_d R^2}{D} f = 0, \quad f'(0) = 0, \quad f(1) = 0,$$

and using  $D = \frac{1}{3}\gamma/k^2(x)$  (the equivalent of the gas kinetic diffusion coefficient  $D = \frac{1}{3}\lambda v$ ). We find

$$\eta\gamma = \nu_d = 1.926\gamma/\tau_x^2.$$

### APPENDIX C: JEFFERIES-WHITE APPROXIMATION

In this appendix the influence on the calculated decay rate due to the Jefferies-White approximation<sup>26</sup> in the redistribution function  $R_{II}(x',x)$  is discussed in more detail.

For large optical thickness the function  $R_{II}(x',x)$  can be approximately written as<sup>26,5</sup>

$$R_{II}(x',x) \simeq L_V(x') [b(x',x)L_D(x) + a(x',x)L_D(x'-x)], \quad (C1)$$

with  $b(x',x) \simeq 1$  and  $a(x',x) \simeq 0$  for  $|x'| \ll x_c$  and, further,  $b(x',x) \simeq 0$  and  $a(x',x) \simeq 1$  for  $|x'| \gg x_c$ . As a function of  $|x'|$ ,  $a(x',x)$  rises from zero to unity for  $|x'|$  near  $x_c$ , the rate of rise depending somewhat on  $|x|$ . The function  $b(x',x)$  behaves complementary. The function  $L_D(x'-x)$  in the second term denotes the Doppler shift experienced in the nonresonant coherent scattering of the photons.

In the approximation first introduced by Jefferies and White,<sup>26</sup> this function is approximated by the  $\delta(x'-x)$  function, and  $R_{II}(x',x)$  is expressed by Eq. (7).<sup>26,5</sup> The function  $a(x')$  in Eq. (7), which is better documented than  $a(x',x)$ , rises strongly for  $|x'|$  near  $x_c$ , as is shown in Ref. 26 [also see Eq. (22)]. In the JW approximation the wing photons can only escape from the volume at their frequency of "creation." Thus the effects of one-dimensional diffusion in frequency space<sup>35,36</sup> from wing frequencies near  $x_c$  to more outward lying optically

thinner frequency regions are neglected. This diffusion process occurs if  $P_c \ll 1$  due to a finite mean frequency shift  $\Delta x_1$ , which is inherent in the scattering term  $L_D(x'-x)$  and because of the larger number of photons emitted with frequency nearer the line core. The mean frequency shift  $\Delta x_1 \simeq 0.7$  (Ref. 36) acts as a mean free path in the diffusion in frequency space. The neglect of this diffusion process causes Eq. (20) to underestimate the decay rate  $\beta$ . For  $x_e < x_c$  ( $n_{\text{Hg}} \lesssim 3 \times 10^{19} \text{ m}^{-3}$ ) the photons emitted in the optically thin wings escape on their first attempt and the approximation has no influence upon the calculated decay rate value.

For  $x_e > x_c$  ( $n_{\text{Hg}} \gtrsim 3 \times 10^{19} \text{ m}^{-3}$ ) a large role in the radiation transport is played by photons in the wings, and the situation is more complicated.

Photons from two sources contribute to the decay rate  $\beta$ .

(i) Photons created in decorrelating collisions ( $\beta_c$ ). Because the term  $P_c L_V(x)$  in the source spectrum  $G(x)$  is a slowly varying function of  $x$  in the wing, and a large fraction of the escaping photons comes from  $x$  values where  $\eta_{\text{eff}} \simeq 1$ , the error in  $\beta_c$  will not be large.

(ii) Photons emitted by the Doppler redistribution ( $\beta_{nc}$ ). This term contributes potentially the largest error to  $\beta$  if the JW approximation is made. It is seen from the behavior of the nonresonant coherent scattering term  $a(x',x)L_D(x'-x)$  in Eq. (C1) that photons scattered by this mechanism to the optically thinner line wing mostly come from the frequency region  $x > x_c$ . For  $x_c \lesssim x_f < x_e$  ( $n_{\text{Hg}} \gtrsim 3 \times 10^{19} \text{ m}^{-3}$ ) the error in  $\beta_{nc}$  increases with increasing mercury density, as long as  $P_c \ll 1$ . Therefore, the error in  $\beta$  will be largest when  $\beta_{nc}$  and  $\beta_c$  of Eq. (21) are about equal ( $n_{\text{Hg}} \simeq 1.5 \times 10^{20} \text{ m}^{-3}$ ), as is confirmed by the data in Fig. 3. With further increasing ground-state density, the error decreases fast. This is because, on one hand, the diffusion length  $\Delta x \simeq \Delta x_1 / (P_c)^{1/2}$  decreases (due to the increasing  $P_c$  value), whereas, on the other hand, the frequency distance  $|x_f - x_c|$  to the effectively optically thin region increases. The chance that a photon will diffuse over a distance  $|x_f - x_c|$ , estimated roughly as

$$\exp \left[ - \left( \frac{x_f - x_c}{\Delta x_1} \right)^2 P_c \right],$$

is about 0.97 for  $n_{\text{Hg}} \simeq 1.5 \times 10^{20} \text{ m}^{-3}$ , but has decreased to about  $1 \times 10^{-3}$  already at  $n_{\text{Hg}} = 6 \times 10^{20} \text{ m}^{-3}$ .

An estimate of the error in  $\beta$  made using the JW approximation is rather difficult and also has to take into account the expressions used for  $a(x')$ ,  $R_{II}(x',x)$ , and  $R_{III}(x',x)$ . From a rough estimation we find that the decay rate  $\beta$  at  $n_{\text{Hg}} = 1.5 \times 10^{20} \text{ m}^{-3}$  is underestimated by about 30% owing to the use of the JW approximation. For this estimation we assumed that in the real situation 50% of the Doppler redistribution photons emitted with  $x > x_c$  diffuse into the line core and 50% into the line wing [i.e., using  $\eta_{\text{eff}} = 0.5$  for  $x > x_c$  in the  $\beta_{nc}$  term of Eq. (20)]. Here,  $x_c$  of the hfs was determined from the equality of the Doppler and Lorentz contributions to the Voigt line profile of the hfs.

\*Present address: Nederlandse Philips Bedrijven B.V., Elcoma Division, Bldg. BE3, P.O. Box 218, 5600 MD Eindhoven, The Netherlands.

- <sup>1</sup>T. Holstein, Phys. Rev. **72**, 1212 (1947); **83**, 1159 (1951).  
<sup>2</sup>L. M. Biberman, Zh. Eksp. Teor. Fiz. **17**, 416 (1947); **19**, 584 (1949).  
<sup>3</sup>M. G. Payne and J. D. Cook, Phys. Rev. A **2**, 1238 (1970).  
<sup>4</sup>C. van Trigt, Phys. Rev. A **13**, 726 (1976).  
<sup>5</sup>M. G. Payne, J. E. Talmage, G. S. Hurst, and E. B. Wagner, Phys. Rev. A **9**, 1050 (1974).  
<sup>6</sup>C. E. Klots and V. E. Anderson, J. Chem. Phys. **56**, 120 (1972).  
<sup>7</sup>C. van Trigt, Phys. Rev. A **13**, 734 (1976).  
<sup>8</sup>M. Koedam, A. A. Kruithof, and J. Riemens, Physica **29**, 565 (1963); B. T. Barnes, J. Appl. Phys. **31**, 852 (1960).  
<sup>9</sup>H. A. Post, J. Phys. B **17**, 3193 (1984).  
<sup>10</sup>C. Kenty, J. Appl. Phys. **9**, 765 (1938).  
<sup>11</sup>K. Murakawa and S. Suwa, J. Phys. Soc. Jpn. **5**, 429 (1950).  
<sup>12</sup>P. van de Weijer and R. M. M. Cremers, J. Appl. Phys. **53**, 1401 (1982).  
<sup>13</sup>B. Klarfeld, Tech. Phys. USSR **5**, 913 (1938); H. T. Saelee, J. Phys. D **15**, 873 (1982).  
<sup>14</sup>P. Laborie, J.-M. Rocard, and J. A. Rees, *Electronic Cross-sections and Macroscopic Coefficients* (Dunod, Paris, 1971), Vol. 2.  
<sup>15</sup>I. V. Semenova and Yu. M. Smirnov, Opt. Spektrosk. **42**, 827 (1977) [Opt. Spectrosc. (USSR) **42**, 477 (1977)].  
<sup>16</sup>H. S. W. Massey, *Electronic and Ionic Impact Phenomena* (Clarendon, Oxford, 1971), Vol. 3, Chap. 8.  
<sup>17</sup>C. Kenty and J. R. Cooper, Trans. Electrochem. Soc. **87**, 397 (1945).  
<sup>18</sup>E. Leboucher, C. Bousquet, and N. Bras, Nouv. Rev. Opt. **5**, 121 (1974). Note that the energy value of the <sup>201</sup>Hg ( $F = \frac{1}{2}$ )

component in MHz units has been misprinted. The correct value should be 8720 MHz. The energy value of the <sup>196</sup>Hg component was obtained using data of S. Gerstenkorn, J. J. Labarthe, and J. Vergès, Phys. Scr. **15**, 167 (1977).

- <sup>19</sup>A. O. Nier, Phys. Rev. **79**, 450 (1950).  
<sup>20</sup>A. V. Phelps, Phys. Rev. **114**, 1011 (1959).  
<sup>21</sup>H. Zanstra, Mon. Not. R. Astron. Soc. **101**, 273 (1941).  
<sup>22</sup>D. L. Huber, Phys. Rev. **178**, 93 (1969); A. Omont, E. W. Smith, and J. Cooper, Astrophys. J. **175**, 93 (1969); G. Nienhuis and F. Schuller, Physica **92C**, 397 (1977); D. Voslamber and J.-B. Yelnik, Phys. Rev. Lett. **41**, 1233 (1978).  
<sup>23</sup>G. Nienhuis, Physica **95C**, 266 (1978).  
<sup>24</sup>W. Unno, Publ. Astron. Soc. Jpn. **4**, 100 (1952).  
<sup>25</sup>D. G. Hummer, Mon. Not. R. Astron. Soc. **125**, 21 (1962).  
<sup>26</sup>J. Jefferies and O. White, Astrophys. J. **132**, 767 (1960).  
<sup>27</sup>P. R. Berman and W. E. Lamb, Phys. Rev. **187**, 221 (1969); A. Omont and J. Meunier, *ibid.* **169**, 92 (1968).  
<sup>28</sup>J. C. Gay, J. Phys. **35**, 813 (1974).  
<sup>29</sup>B. Davison, *Neutron Transport Theory* (Clarendon, Oxford, 1957), Chaps. 1–8.  
<sup>30</sup>A. Lurio, Phys. Rev. **140**, A1505 (1965).  
<sup>31</sup>W. Gautschi, SIAM J. Num. Anal. **7**, 187 (1970).  
<sup>32</sup>H. A. Post, P. van de Weijer, and R. M. M. Cremers, following paper, Phys. Rev. A **33**, 2017 (1986).  
<sup>33</sup>I. S. Gradshteyn and I. M. Ryzhik, *Table of Integrals, Series and Products* (Academic, New York, 1956), p. 92.  
<sup>34</sup>*Handbook of Mathematical Functions*, edited by M. Abramowitz and I. A. Stegun (U.S. GPO, Washington, D. C., 1972), p. 369.  
<sup>35</sup>W. Unno, Publ. Astron. Soc. Jpn. **7**, 81 (1955).  
<sup>36</sup>D. E. Osterbrock, Astrophys. J. **135**, 195 (1962).